Journal of Power Sources 241 (2013) 627–633

Contents lists available at SciVerse ScienceDirect

Journal of Power Sources

journal homepage: www.elsevier.com/locate/jpowsour

Ti-doped molybdenum-based perovskites as anodes for solid oxide fuel cells

Beibei He [a], Zhenbin Wang [a], Ling Zhao [b], Xin Pan [a], Xiaojun Wu [a], Changrong Xia [a,*]

[a] CAS Key Laboratory of Materials for Energy Conversion, Department of Materials Science and Engineering, University of Science and Technology of China, Hefei 230026, Anhui, China
[b] Fuels and Energy Technology Institute, Curtin University, Perth 6102, WA, Australia

HIGHLIGHTS

- $Sr_2Ti_{2x}Ni_{1-x}Mo_{1-x}O_6$ (x = 0, 0.1, 0.3, 0.5, 0.7) perovskites are synthesized.
- The strong Ti–O bond is held responsible for the enhanced structural stability.
- First-principle calculations are performed on the conduction properties.
- Cells with $Sr_2TiNi_{0.5}Mo_{0.5}O_6$ anode show remarkable carbon tolerance.

GRAPHICAL ABSTRACT

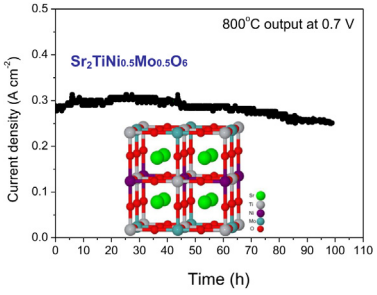

ARTICLE INFO

Article history:
Received 23 November 2012
Received in revised form
27 April 2013
Accepted 29 April 2013
Available online 14 May 2013

Keywords:
Solid oxide fuel cells
Ceramic anodes
Conductivity
Electrochemical performance
Ti-doping

ABSTRACT

Ti doping is found to increase the stability of Sr_2NiMoO_6 perovskite oxides in reducing atmosphere. The composition $Sr_2TiNi_{0.5}Mo_{0.5}O_6$ (STNM) is further evaluated as a potential oxide anode for solid oxide fuel cells (SOFCs). Electrical conductivity, thermal expansion coefficient, surface exchange coefficient, chemical diffusion coefficient, and its electrochemical performance in single cells with $La_{0.8}Sr_{0.2}Ga_{0.8}Mg_{0.2}O_{3-\delta}$ (LSGM) electrolytes are investigated. STNM exhibits a high conductivity of 17.5 S cm^{-1} at 800 °C at anodic atmosphere. The material shows good chemical and thermal expansion compatibilities with LSGM. To investigate the effect of Ti doping on the conduction properties, first-principle calculations are performed using the Vienna Ab initio Simulation. The strong Ti–O bond is held responsible for the enhanced structural stability of STNM under humidified H_2 atmospheres, relative to that of the undoped system. The remarkable cell performance with both H_2 and dry CH_4 as the fuel indicates the potential ability of STNM to be used as SOFC anodes. These results obtained indicate that $Sr_2TiNi_{0.5}Mo_{0.5}O_6$ is a promising material for use as anode for intermediate temperature SOFCs.

1. Introduction

The traditional Ni-based cermet anode, which works well with H_2 fuel, has been extensively studied over the years to provide high performance for solid oxide fuel cells (SOFCs). However, Ni is susceptible to degradation by sulfur poisoning, coking, segregation of other impurities at the three-phase boundaries, coarsening, and can be severely damaged by redox cycles due to the occurrence of Ni–NiO phase transitions [1–4]. On the other hand, anodes entirely composed of ceramic oxides offer a number of potential advantages over metals, such as mixed ionic–electronic conductivity, redox stability and fine microstructures. To operate efficiently for a commercially viable lifetime, such an anode catalyst must satisfy the following requirements: high electro-oxidation activity, sulfur tolerance, coking resistance, redox stability, and high electronic and ionic conductivity [5].

From this point of view, much of the efforts have been directed toward ABO_3 perovskites, which can offer general stability, high

* Corresponding author. Tel.: +86 551 3607475; fax: +86 551 3601592.
E-mail address: xiacr@ustc.edu.cn (C. Xia).

0378-7753/$ – see front matter © 2013 Elsevier B.V. All rights reserved.
http://dx.doi.org/10.1016/j.jpowsour.2013.04.148

electronic conductivity, and are flexible toward substitution with dopants [6]. Many perovskites have been investigated as potential anode materials, mainly chromite- and titanate-based perovskites such as $(La_{1-x}Sr_x)_{0.9}Cr_{0.5}Mn_{0.5}O_{3-\delta}$ [7,8], and doped strontium titanium oxides [3,9]. However, the electrical conductivity of $(La_{1-x}Sr_x)_{0.9}Cr_{0.5}Mn_{0.5}O_{3-\delta}$ is relatively low. La-substituted $SrTiO_3$ materials show high electrical conductivity in reducing atmosphere as well as chemical stability, but their electrocatalytic activity is insufficient. Recently, molybdenum-based double perovskites Sr_2MMoO_6 (M = Mg, Mn, Fe, Co, and Ni) have been explored as the anodes operating well with both H_2 and CH_4 fuels [4,10–13]. It is known that the 3d-block transition metals, such as Fe, Co and Ni normally exhibit high catalytic activity for the oxidation of H_2 and CH_4. Among these molybdenum-based oxides, Sr_2NiMoO_6 exhibits notable electrochemical performance even in dry CH_4 atmospheres [4]. Although an increased catalytic activity for methane cracking is observed upon substitution of the transition metals in Sr_2NiMoO_6, a concomitant decrease of its stability is noted [14]. It has been reported that Ni containing perovskites are unstable at low oxygen partial pressures, leading to segregation of the metal [15–17]. The poor stability under reducing atmospheres is due to a weakening of the bond between nickel and oxygen.

Fortunately, the stability of SNM can be improved by partial substitution [18,19]. For example, Graves et al. [17] have found that adding Ti to the B-site prevents Sr_2NiMoO_6 from decomposition in reducing atmosphere. The crystal structure retains stable, which can be associated with the smaller ionic radius of Ti^{4+} ions (60.5 pm) relative to that of Ni^{2+} (69 pm) and Mo^{6+} ions (65 pm). Furthermore, electronic conduction occurs as a consequence of the valence change of Ti^{4+} to Ti^{3+}, following the release of oxygen and the concomitant formation of oxygen vacancies at high temperatures (>300 °C) in reducing atmospheres. For the series $La_{0.75}Sr_{0.25}Cr_{0.5}X_{0.5}O_{3-\delta}$ (X = Fe, Ti, Mn) oxides, Danilovic et al. [20] observed the highest electrode performance in 0.5% H_2S/CH_4 fuel for the Ti substituted material. These results suggest that Ti substitution might improve the electrochemical activity of oxide anodes.

Much of the research into SOFC anode materials is a delicate balance between obtaining high performance and reliable stability. In this work, we consider the advantages of both Sr_2NiMoO_6, which shows a high catalytic activity, and $SrTiO_3$, which is stable under anodic conditions, and report the effects of Ti doping on the crystal structure and phase stability of $Sr_2Ti_{2x}Ni_{1-x}Mo_{1-x}O_6$ ($x = 0$, 0.1, 0.3, 0.5 and 0.7) in reducing atmosphere. Electrical conductivities and electrochemical performance of the composition $x = 0.5$, $Sr_2TiNi_{0.5}Mo_{0.5}O_6$, are investigated as anode for the SOFC. Moreover, the density of state (DOS) of Sr_2NiMoO_6 and $Sr_2TiNi_{0.5}Mo_{0.5}O_6$ is studied by means of first principles calculations.

2. Experimental

2.1. Powders preparation and cell fabrication

The materials used in this work include $Sr_2Ti_{2x}Ni_{1-x}Mo_{1-x}O_6$ ($x = 0$, 0.1, 0.3, 0.5 and 0.7), $La_{0.8}Sr_{0.2}Ga_{0.8}Mg_{0.2}O_{3-\delta}$ (LSGM, the electrolyte), $Sm_{0.5}Sr_{0.5}CoO_3$ (SSC, the cathode) and $Sm_{0.2}Ce_{0.8}O_{1.9}$ (SDC, cathode additive). $Sr_2Ti_{2x}Ni_{1-x}Mo_{1-x}O_6$ powders were synthesized by a sol–gel assisted combustion method. All starting chemicals were of analytical grade and obtained from Sinopharm Chemical Reagent Co., Ltd. Tetrabutyl titanate, $Sr(NO_3)_2$, $Ni(NO_3)_2 \cdot 6H_2O$ and $(NH_4)_6Mo_7O_{24} \cdot 4H_2O$ were used as metal precursors and dissolved in distilled water. Citric acid and acetic acid were used to adjust the pH in order to prevent precipitation, while glycine was used as the fuel for combustion. After stirring for a few hours, the solution was heated until self-ignition. The combustion product, dark ash, was collected and subsequently calcined at 600 °C for 5 h and then 1200 °C for 10 h to remove any organic residues and to obtain the desired cubic phase. SSC and SDC powders were synthesized via the glycine–nitrate process [21]. LSGM powders were synthesized through the citric acid–EDTA process as earlier reported by Wang et al. [22].

LSGM substrates were formed by dry-pressing the LSGM powder uniaxially under 200 MPa. The pellets, 15 mm in diameter, were then sintered at 1450 °C in air for 5 h to form dense electrolytes, about 0.6 mm thick. Electrolyte-supported single cells, consisting of LSGM electrolyte, $Sr_2TiNi_{0.5}Mo_{0.5}O_6$ (STNM) anode, and SSC–SDC cathodes were fabricated for electrochemical investigation. To prepare the anode, an ink consisting of STNM, graphite and terpineol was applied to one side of the LSGM surface using a screen-printing method, and subsequently fired at 1200 °C in air for 3 h to form porous electrodes. The resulting anodes were about 60 μm thick having an area similar to that of the electrolyte substrate. The screen-printing method was also applied for the cathode. SSC–SDC powders with 30 wt.% SDC were grounded with 10 wt.% ethylcellulose–terpineol binder to make cathode slurry. The slurry was then painted on the other side of the LSGM electrolyte surface, and subsequently fired at 950 °C for 2 h to form the SSC–SDC cathode. The effective cathode area was 0.24 cm^2.

2.2. Material characterization

Phase identification was conducted by X-ray diffraction (XRD, Philips X'pert PROS diffractometer) analysis using CuKα radiation (D/Max-gA) at room temperature. The commercially available software Jade was used for identification of the phases. To examine the chemical compatibility with the electrolyte, the prepared STNM powder, which was confirmed to exhibit a pure perovskite structure, was mixed with LSGM in the weight ratio of 1:1, pressed to pellets, and calcined at 1300 °C for 10 h in air. The calcined pellets were crushed and examined using XRD to clarify the phase purity. The microstructure was revealed via a scanning electron microscope (SEM, JSM-6700F, JEOL).

Spin polarized Density Functional Theory (DFT) calculations were carried out by using the Vienna Ab initio Simulation Package (VASP) with the projector-augmented wave method [23]. The structure model of $Sr_2TiNi_{0.5}Mo_{0.5}O_6$ is constructed according to the experimental cubic structure of Sr_2NiMoO_6 [24]. The optimized structure of Sr_2NiMoO_6 is illustrated in Fig. 1a. The random doping of Ti atom on the B site of Sr_2NiMoO_6 leads to numerous possible arrangements. Munoz-Garcia [25] reported that the distribution of doped atoms on the high symmetrical site is a most stable structure. Thus, in order to simplify the calculation, a structure that B site atoms were homogeneously distributed was considered, as shown in Fig. 1b. The exchange correlation effects were treated employing the generalized gradient approximation (GGA) with the Perdew–Burke–Ernzerhof (PBE) functional [26]. The kinetic energy cutoff for a plane-wave basis set was 520 eV. The structural relaxations are performed until the force on each atom lower than 0.01 eV $Å^{-1}$. The Brillouin-zone integration based on the Monkhorst–Pack [27] scheme with $(8 \times 8 \times 8)$ k points was carried out. Ferromagnetic state was used and all calculations were spin polarized.

2.3. Electrochemical characterization

Electrical conductivity was measured from 400 to 800 °C in oxidizing and reducing (using a hydrogen/carbon dioxide buffered gas system) atmospheres using a dc current four-probe method. Thermal expansion coefficient (TEC) was measured in the temperature range from 20 to 1200 °C using a dilatometer (SHIMADZU50) at a heating rate of 10 °C min^{-1}. The pressed green bar was first sintered at 1450 °C for 5 h, and then reduced at 800 °C in wet H_2 (3% H_2O) for 10 h for conductivity and TEC measurements.

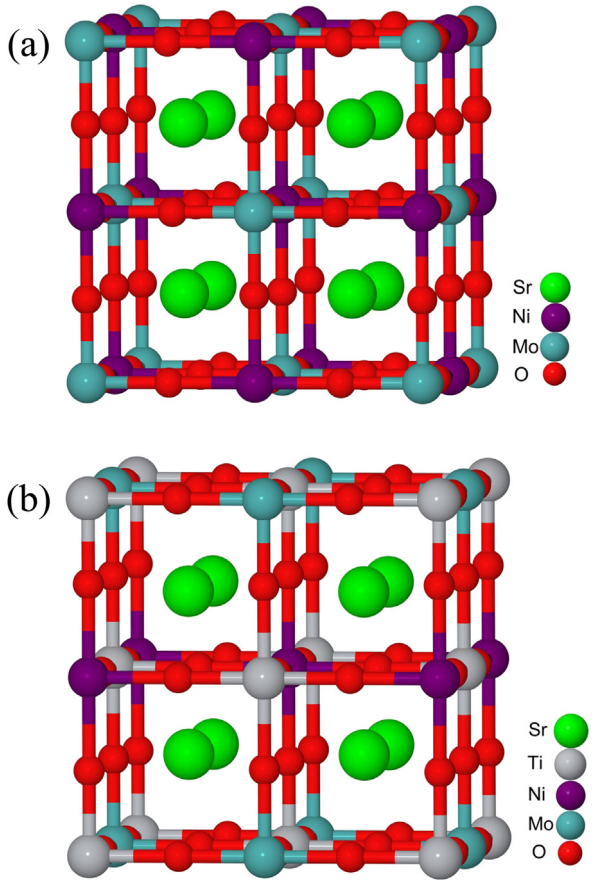

Fig. 1. Schematic representation of the structure of (a) Sr_2NiMoO_6; and (b) $Sr_2TiNi_{0.5}Mo_{0.5}O_6$. Atom (color): Sr (lime), Ti (light gray), Ni (purple), Mo (dark turquoise), O (red). (For interpretation of the references to color in this figure legend, the reader is referred to the web version of this article.)

Bar specimens (approximately 14.00 × 5.05 × 0.60 mm) were also prepared for the measurement of the surface exchange coefficient (k_{ex}) and chemical diffusion coefficient (D_{chem}) in reducing atmospheres. STNM powders were isostatically pressed into a rectangular bar followed by sintering at 1450 °C for 5 h, resulting in relative density over 98% as determined using the Archimedes method. k_{ex} and D_{chem} were obtained by performing electrical conductivity relaxation (ECR) measurements [28]. During measurement, at 800 °C, the electrical conductivity after an instantaneous change of the oxygen partial pressure from 3.7×10^{-22} to 1.3×10^{-22} atm was recorded using a dc four-probe technique.

Single cells were sealed onto alumina tubes. Ag paste (DAD-87, Shanghai Research Institute of Synthetic Resins) and Ag wires were used to ensure the electronic contact. Humidified (3% H_2O) hydrogen was used as the fuel with a flow rate of 50 mL min^{-1} and ambient air as the oxidant. An electrochemical workstation (IM6e, Zahner) was used to characterize the single cells. The current–voltage curve was measured by using a galvanostat mode and the electrochemical impedance spectra were obtained under open circuit conditions in the frequency range typically from 0.1 Hz to 1 MHz.

3. Results and discussion

3.1. Phase development and stability

As determined by XRD, all of the $Sr_2Ti_{2x}Ni_{1-x}Mo_{1-x}O_6$ ($x = 0$, 0.1, 0.3, 0.5 and 0.7) powders calcined in air at 1200 °C have shown the formation of a cubic perovskite-type structure, which is in good qualitative agreement with those of Co-doped $Sr_2Fe_{1.5}Mo_{0.5}O_6$ oxides [29]. Because the mixed-conducting oxides used as anodes should be stable under SOFC operating environments, all of the powders were reduced at 800 °C for 10 h in hydrogen stream containing 3% H_2O. As shown in Fig. 2b, undoped Sr_2NiMoO_6 is found not to be stable under this reducing condition. It decomposes to multiple compounds, including $SrMoO_3$, Sr_3MoO_6, Sr_2MoO_4, Ni, and $MoNi_4$. This is in agreement with the previous observations [17]. When the doping content is $x = 0.1$ and 0.3, the stability seems to be improved, but the samples are still not fully stabilized. When the dopant content increases to $x = 0.5$ and 0.7, no obvious phase change is observed, suggesting these two samples are stable. The structural stability of perovskite oxides is primarily related with the stability of the BO_6 octahedra. So, the improved stability of the oxides with $x = 0.5$ and 0.7 under reducing environment is probably due to the strong bond energy between titanium and oxygen. The calculated lattice parameters of $Sr_2TiNi_{0.5}Mo_{0.5}O_6$ and $Sr_2Ti_{1.4}Ni_{0.3}Mo_{0.3}O_6$ in air are 7.843(4) Å and 7.824(8) Å, respectively. After annealing in the hydrogen stream, the cell parameters increase slightly. This is possibly due to the decrease in oxygen stoichiometry and concomitant increase of the cation radius as a result of Ti^{4+} reduction.

3.2. Electrical characteristics

Samples with $x = 0.5$ and 0.7 were selected for conductivity measurements as these were found to be stable in reducing

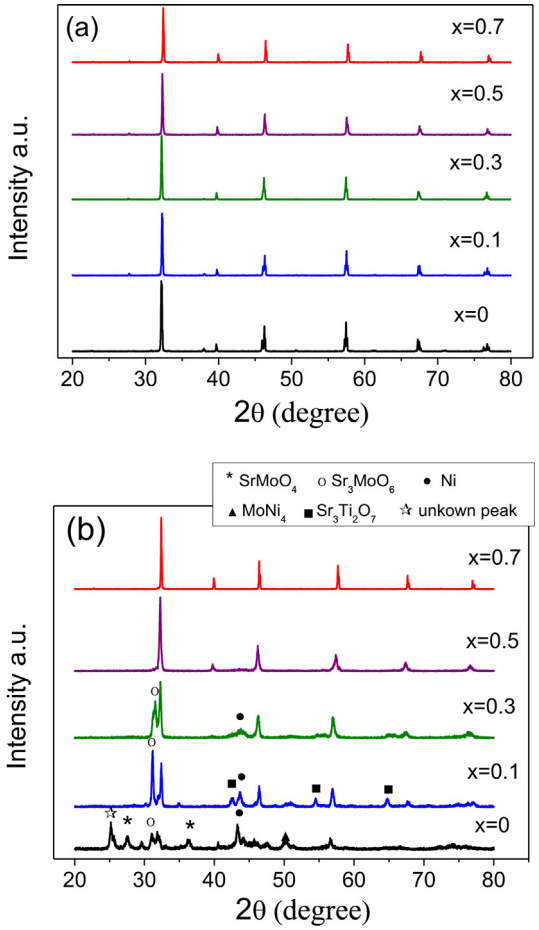

Fig. 2. XRD patterns of $Sr_2Ti_{2x}Ni_{1-x}Mo_{1-x}O_6$ ($x = 0$, 0.1, 0.3, 0.5, 0.7) (a) sintered at 1200 °C for 10 h in air and (b) sintered at 1200 °C for 10 h in air and then reduced at 800 °C in H_2 (3% H_2O)/Ar for 10 h.

atmosphere, as discussed above. Fig. 3a shows data of electrical conductivity as a function of temperature measured in humidified (~3% H_2O) hydrogen. The conductivity for $x = 0.5$ is found to be much higher than that for $x = 0.7$. For this reason, the composition with $x = 0.5$ was chosen for further investigation as anode material.

At 800 °C, $Sr_2TiNi_{0.5}Mo_{0.5}O_6$ (STNM) shows a conductivity of 17.5 S cm^{-1}, suggesting that STNM meets the requirement of anode material operating in the range for intermediate-temperature SOFCs (600–800 °C) [30]. The observed metal-like behavior shown in Fig. 3a is similar to that observed for of $SrTiO_3$ prepared by sintering in a reducing environment [9,31,32]. The electrical conductivity STNM can be ascribed to the electron delocalization associated with the covalent nature of the $-Mo^{6+}-O-Ti(Ni)-O-Mo^{5+}-$ bond. It may be noted that the conductivity is higher than that found for $La_{0.75}Sr_{0.25}Cr_{0.5}Mn_{0.5}O_3$ (1.5 S cm^{-1} at 900 °C in 5% H_2/Ar) and $Sr_2MgMoO_{6-\delta}$ (9.3 S cm^{-1} at 800 °C in H_2) [7,10], but lower than that found for $Sr_{0.86}Y_{0.08}TiO_3$ (82 S cm^{-1} at 800 °C and oxygen partial pressure of 10^{-19} atm) and $La_{0.4}Sr_{0.6}TiO_3$ (360 S cm^{-1} at 1000 °C and oxygen partial pressure of 10^{-18} atm) [3,9]. However, the $SrTiO_3$ based oxides must be prepared under reducing atmosphere to achieve high electrical conductivity. On the contrary, STNM can be synthesized in air, which is preferred from a manufacturing point of view.

Fig. 3b shows the electrical conductivity at various oxygen partial pressures, P_{O2}. The conductivity decreases with increasing P_{O2}. The power dependence is negative, and takes values between −1/6 and −1/4, indicating n-type conductivity. The conductivity is 18 S cm^{-1} at $P_{O2} = 10^{-22}$ atm. It is only 0.03 S cm^{-1} when the P_{O2} increases to 10^{-8} atm. The high conductivity can be regained in reducing atmosphere after being exposed to an oxidizing environment. It suggests that STNM is a potential anode material which is stable against redox cycling.

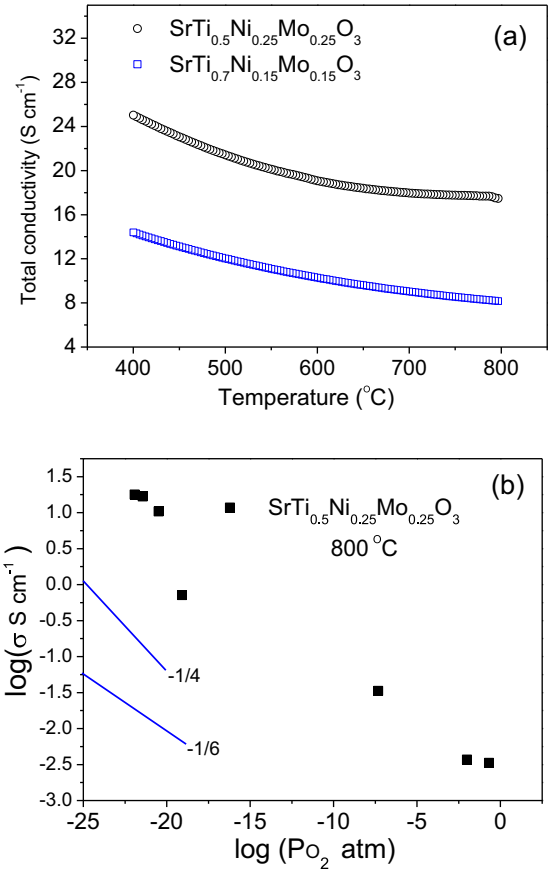

Fig. 3. Electrical conductivity of (a) $Sr_2Ti_{2x}Ni_{1-x}Mo_{1-x}O_6$ ($x = 0.5$ and 0.7) as a function of temperature. (b) $Sr_2TiNi_{0.5}Mo_{0.5}O_6$ at different oxygen pressures.

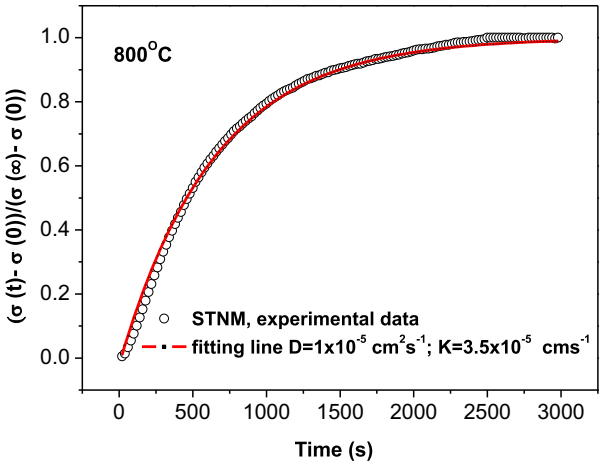

Fig. 4. Experimental and fitting profiles of the conductivity for $Sr_2TiNi_{0.5}Mo_{0.5}O_6$ at 800 °C as a function of relaxation time.

Fig. 4 shows the conductivity relaxation profiles at 800 °C for STNM bar sample undergoing a sudden oxygen partial pressure

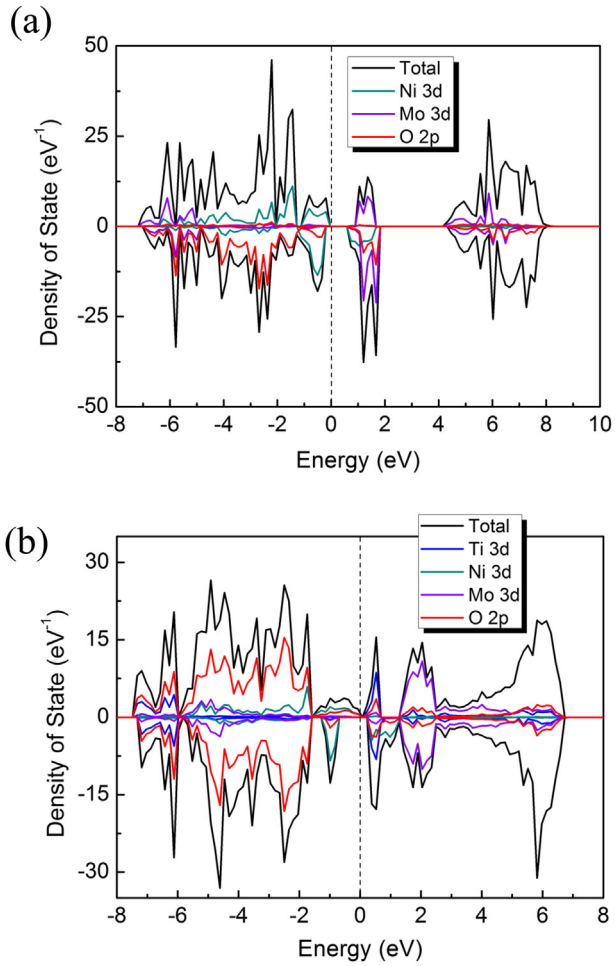

Fig. 5. Partial densities of states diagrams for (a) Sr_2NiMoO_6; (b) $Sr_2TiNi_{0.5}Mo_{0.5}O_6$. Zero level corresponds to the Fermi energy.

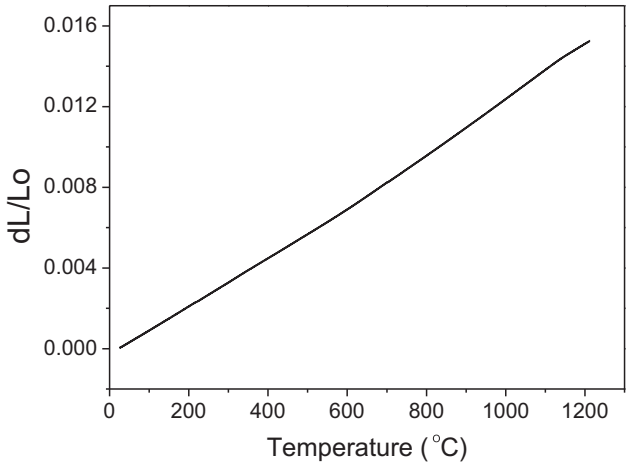

Fig. 6. Thermal expansion curves for $Sr_2TiNi_{0.5}Mo_{0.5}O_6$.

change from 3.7×10^{-22} to 1.3×10^{-22} atm. The re-equilibration time is about 3000 s, at which the normalized conductivity is stabilized. By fitting the experimental data with Fick's second law, k_{ex} of the STNM sample is determined to be 3.5×10^{-5} cm s^{-1}. The ECR method also allows the determination of chemical diffusion coefficient (D_{chem}), which is about 1.0×10^{-5} cm^2 s^{-1} at 800 °C. The ratio of D_{chem}/k_{ex} is approximately 0.3 cm, which is close to the sample dimensional to obtain reliable requirement for reliable results [33].

In order to gain insight into the effect of Ti doping on the electrical conduction behavior, first-principles calculations were carried out based on Density Functional Theory (DFT) [34]. As one can see in Fig. 5, the densities of states (DOSs) of the two oxides are obviously different. Sr_2NiMoO_6 (Fig. 5a) exhibits a typical semiconductor property with a band gap. This result is consistent with previous studies by Gagulin et al. [35], who reported that the conductivity of Sr_2NiMoO_6 exhibited semiconducting behavior. However, no band gap in $Sr_2TiNi_{0.5}Mo_{0.5}O_6$ (Fig. 5b) is observed. A donor level is formed on account of Ti-doping, causing the Fermi level to move closer to the valence band. Therefore, a much smaller band gap formed in $Sr_2TiNi_{0.5}Mo_{0.5}O_6$, which is propitious to the electron conduction and thus decreases the activation energy of electron conductivity [36]. Besides, Ti doping induces additional peaks in the energy range at 2–4 eV where no states are observed in Sr_2NiMoO_6 crystal. The main contribution to the additional DOS peaks comes from additional B-site Ti cation. The DOS of d electrons of the B-site ions around the Fermi level overlap with the oxygen 2p electrons, which may indicate an increase in charge carrier concentration. All the cases imply that $Sr_2TiNi_{0.5}Mo_{0.5}O_6$ is a good electronic conductor. Moreover, $Sr_2TiNi_{0.5}Mo_{0.5}O_6$ as well as Sr_2NiMoO_6 oxides are proved to be ferromagnetic due to the asymmetric DOS.

3.3. Thermal expansion and chemical compatibilities

The thermal expansion compatibility of the anode material with the electrolyte is critical for the SOFC. Poor matching of their TECs may induce exfoliation of the electrodes during fabrication and/or operation, and hence shorten the lifetime of the SOFC. The thermal expansion curve for STNM is shown in Fig. 6. In the temperature range of 20–1300 °C, the average TEC is 12.8×10^{-6} K^{-1}, which is very close to the value of $12–13 \times 10^{-6}$ K^{-1} observed for the LSGM electrolyte [37,38]. It is noted that the coefficient is also close to the TEC of undoped Sr_2NiMoO_6, 12.9×10^{-6} K^{-1}, indicating that Ti doping does not noticeably affect the thermal expansion of Sr_2NiMoO_6. Additionally, XRD analysis revealed no new phases in the STNM/LSGM mixture after sintering at 1300 °C. The results show that STNM has a good chemical compatibility with LSGM. To this end, LSGM was chosen as the electrolyte for fuel cell testing.

3.4. Cell performance and carbon tolerance

The cross-sectional view of the electrolyte-supported cell equipped with the STNM anode after electrochemical testing is presented in Fig. 7. The cell consists of a 700 μm thick LSGM electrolyte, a 60 μm thick STNM single phase anode and a 30 μm thick SSC–SDC composite cathode. The electrolyte is fully dense, and all electrodes show high porosity and a good adherence to the electrolyte, ensuring a low contact resistance between the anode and electrolyte. Fig. 7b demonstrates that the STNM anode is composed of uniform particles and pores. The particle size ranges between 2 and 4 μm. Since 10 wt.% pore performer was added to the STNM anode ink, some larger pores can be observed in the anode structure.

The properties of double perovskite oxides are strongly affected by the constituent B-site cations, such as their ratio and the degree of cation ordering [10,39]. It has been found that both the Mo content and the presence of intrinsic oxygen vacancies play important roles in the catalytic activity of $Sr_2Fe_xMo_{2-x}O_6$ [39–41]. In order to elucidate the influence of B-site doping of SNM by titanium, the performance of the STNM anode was tested using LSGM electrolyte-supported single cells with SSC–SDC as the cathode. *I–V* and *I–P* curves obtained at different temperatures with H_2 as the fuel and ambient air as the oxidant are shown in

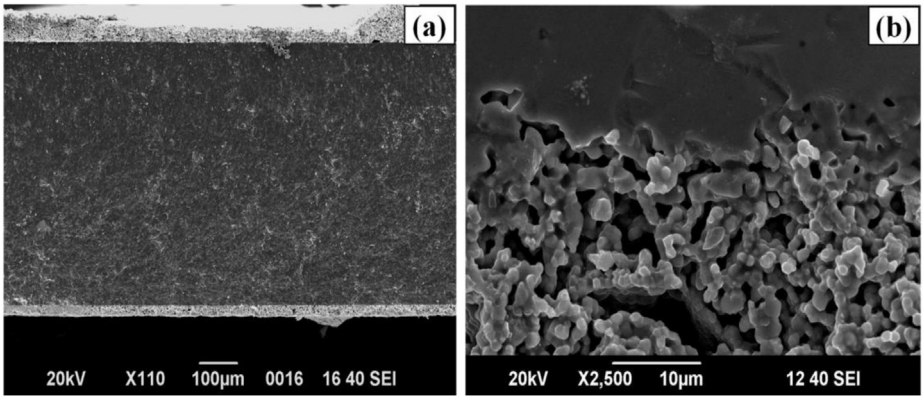

Fig. 7. SEM images of (a) cross-sectional view of the cell, and (b) $Sr_2TiNi_{0.5}Mo_{0.5}O_6$ anode and electrolyte interface.

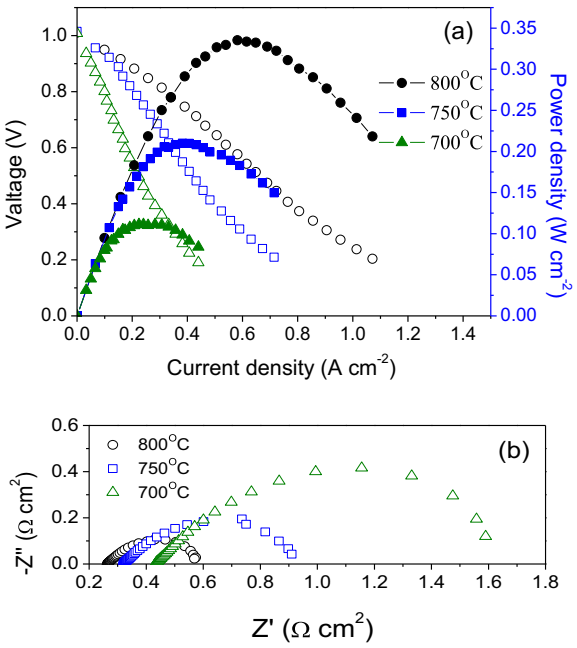

Fig. 8. (a) Typical *I–V* and *I–P* curves measured at 800 °C for single cells based on $Sr_2TiNi_{0.5}Mo_{0.5}O_6$ anode with humidified H_2 as the fuel and ambient air as the oxidant, and (b) impedance spectra of the cell measured under open circuit conditions.

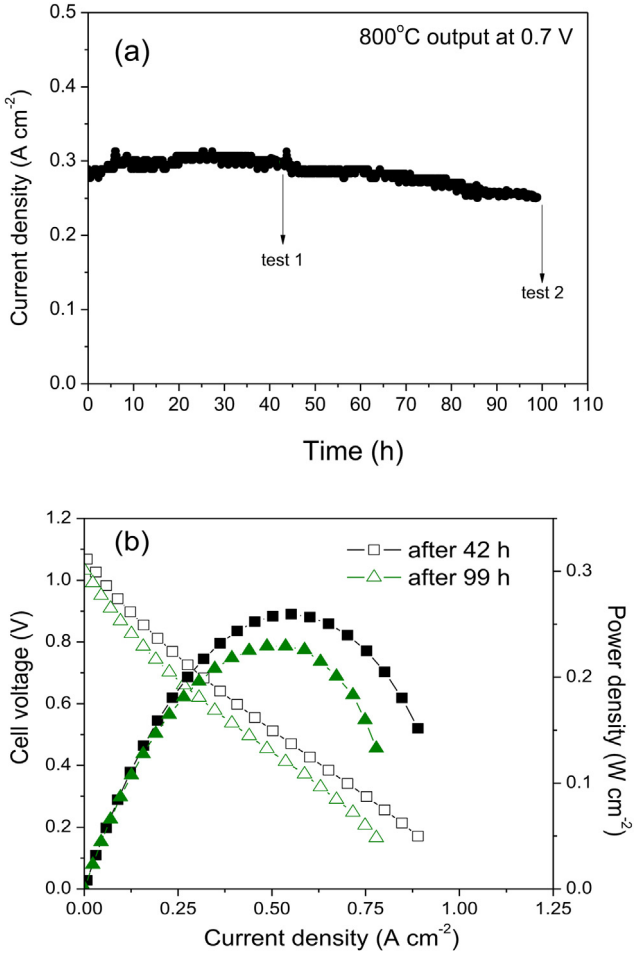

Fig. 9. (a) Endurance test for the cell with $Sr_2TiNi_{0.5}Mo_{0.5}O_6$ anode in dry CH_4 with a fixed potential of 0.7 V at 800 °C, and (b) *I–V* and *I–P* curves measured after 42 and 99 h life test, respectively.

Fig. 8a. It can be seen that the peak power densities are 111, 210, and 335 mW cm^{-2} at 700, 750, and 800 °C, respectively. The impedance spectra of the single cell obtained under open-circuit conditions at different temperatures are shown in Fig. 8b. The interfacial polarization resistance is 0.305 Ω cm^2 at 800 °C, which is higher than that of $SrFe_{2/3}Mo_{1/3}O_3$ anode in a single cell with $La_{0.6}Sr_{0.4}Co_{0.2}Fe_{0.8}O_3$ as the cathode (~0.2 Ω cm^2 at 800 °C) [41], while it is lower than that of $La_{0.7}Sr_{0.3}TiO_3$ anode measured with $La_{0.8}Sr_{0.2}FeO_3$–$Y_{0.08}Zr_{0.92}O_{1.96}$ (LSF–YSZ) as the cathode (~0.5 Ω cm^2 at 900 °C) [42].

To test the performance stability of the STNM anode in the presence of methane, the cell was tested in dry CH_4 with a fixed potential of 0.7 V at 800 °C. As shown in Fig. 9a, the current density remains fairly stable for 24 h, and then starts to decline, from 283 mA cm^{-2} to 252 mA cm^{-2} within 99 h. The slight degeneration observed in the performance might originate from the poor stability of the cobalt-based cathode [43].

During operation of the cell, after 42 and 99 h, additional tests were conducted in which *I–V* and *I–P* curves were recorded with dry CH_4 as the fuel. Prior to these tests, the cell was kept at open circuit condition for 1 h. Corresponding results are shown in Fig. 9b. The open circuit voltage is 1.07 V after 42 h and 1.03 V after 99 h operation, close to the theoretical value. The peak power density is 259 mW cm^{-2} after 42 h operation at 800 °C. The peak power density using dry CH_4 as the fuel is 77.3% of that using H_2 as the fuel at 800 °C. There is a 22.7% reduction in the performance when the fuel is changed from H_2 to dry methane. However, the reduction is much lower than that achieved with typical oxide anodes. For instance, using $Sr_2Fe_{1.5}Mo_{0.5}O_6$ as the anode, the peak cell power density at 850 °C with CH_4 as the fuel is only 125 mW cm^{-2}, while it is 580 mW cm^{-2} with H_2 as the fuel [44], indicating a 78.5% reduction in power density. With a $La_{0.75}Sr_{0.25}Cr_{0.50}Mn_{0.50}O_3$-based ceramic anode, the reduction is about 57.5%, which value can be calculated from reported values of 0.47 W cm^{-2} for H_2 and 0.2 W cm^{-2} for CH_4 at 900 °C [45]. It is further noted that the performance reduction observed in this study is almost equal to the 23.4% power density drop, at 600 °C, observed for a Ni-based cell, comprising Ni–SDC anodes, SDC thin film electrolyte and SSC–SDC cathodes, after a similar change in fuel [46]. The low performance drop upon switching of the fuel from H_2 to CH_4 can be attributed to the relatively high electrocatalytic activity of STNM for the reaction of the hydrocarbon with oxide ions at the three phase boundary (TPB) [47]. The high open circuit voltage and relatively low reduction in peak power density observed from fuel changing demonstrate that with Ti-doping, STNM balances both stability in anode atmosphere and electrocatalytic active. These results suggest that STNM is a promising material for use as anode in IT-SOFCs for direct utilization of hydrocarbon fuels.

4. Conclusions

Ti-doped molybdenum-based double perovskites, $Sr_2Ti_{2x}Ni_{1-x}Mo_{1-x}O_6$ (x = 0, 0.1, 0.3, 0.5 and 0.7) have been synthesized by the sol–gel assisted combustion method. Doping with titanium is found to improve the stability of materials under reducing atmospheres. The composition $Sr_2TiNi_{0.5}Mo_{0.5}O_6$ (STNM) was selected for investigation as anode for the SOFC. The materials were studied with regard to their chemical stability, thermal and chemical compatibility with the LSGM electrolyte, electronic conductivity, surface exchange and chemical diffusion coefficients, and electrochemical performance. At 600–800 °C, its conductivity is found to 17–20 S cm^{-1}, fulfilling the conductivity requirement for use as anode. The thermal expansion coefficient is close to that of LSGM. In addition, STNM is found to be chemically compatible

with LSGM at temperatures below 1300 °C. The single cell with an STNM anode, LSGM electrolyte and SSC–SDC cathode generates, at 800 °C, a peak power density of 335 mW cm^{-2}, and interfacial polarization resistance of 0.305 Ω cm^2. The STNM anode is found to exhibit relatively stability over the test period, 99 h, in using dry methane as the fuel. The present results clearly suggest that $Sr_2TiNi_{0.5}Mo_{0.5}O_6$ is a promising material for use as anode in IT-SOFCs for direct utilization of hydrocarbon fuels. The electrochemical process of direct utilization of methane needs to be further investigated.

Acknowledgments

We thank gratefully acknowledge the financial support of the Ministry of Science and Technology of China (2012CB215403) and Specialized Research Fund for the Doctoral Program of Higher Education (20113402110014). The authors acknowledge Supercomputing Center of USTC and National Supercomputing Center in Tianjin for providing computational resources.

References

[1] B.C.H. Steele, I. Kelly, H. Middleton, R. Rudkin, Solid State Ionics 28–30 (1998) 1547.
[2] Y. Matsuzaki, I. Yasuta, Solid State Ionics 132 (2000) 261.
[3] O.A. Marina, N.L. Canfield, J.W. Stevenson, Solid State Ionics 149 (2002) 21.
[4] Y.H. Huang, R.I. Dass, J.C. Denyszyn, J.B. Goodenough, J. Electrochem. Soc. 153 (2006) A1266.
[5] M.D. Gross, J.M. Vohs, R.J. Gorte, J. Mater. Chem. 17 (2007) 3071.
[6] P.I. Cowin, C.T.G. Petit, R. Lan, J.T.S. Irvine, S.W. Tao, Adv. Energy Mater. 1 (2011) 314–332.
[7] S.W. Tao, J.T.S. Irvine, Nat. Mater. 2 (2003) 320.
[8] D.M. Bastidas, S.W. Tao, J.T.S. Irvine, J. Mater. Chem. 16 (2006) 1603.
[9] S.Q. Hui, A. Petric, J. Electrochem. Soc. 149 (2002) J1.
[10] Y.H. Huang, R.I. Dass, Z.L. Xing, J.B. Goodenough, Science 312 (2006) 254.
[11] Y.H. Huang, G. Liang, M. Croft, M. Lehtimaki, M. Karppinen, J.B. Goodenough, Chem. Mater. 21 (2009) 2319–2326.
[12] S. Colis, D. Stoeffler, C. Mény, T. Fix, C. Leuvrey, G. Pourroy, A. Dinia, P. Panissod, J. Appl. Phys. 98 (2005) 033905.
[13] Z.M. Wang, Y. Tian, Y.D. Li, J. Power Sources 196 (2011) 6104.
[14] C. Li, W. Wang, N. Zhao, Y. Liu, B. He, F. Hu, C. Chen, Appl. Catal. B 102 (2011) 87.
[15] T. Nakamura, G. Petzow, L. Gauckler, J. Mater. Res. Bull. 14 (1979) 649.
[16] R.T. Baker, I.S. Metcalfe, Appl. Catal. A 126 (1995) 319.
[17] C. Graves, B.R. Sudireddy, M. Mogensen, ECS Trans. 28 (2010) 173.
[18] S.W. Tao, J.T.S. Irvine, Adv. Mater. 17 (2005) 1734.
[19] Q. Zeng, Y.B. Zuo, C.G. Fan, C.S. Chen, J. Membr. Sci. 335 (2009) 140.
[20] N. Danilovic, A. Vincent, J. Luo, K.T. Chuang, R. Hui, A.R. Sanger, Chem. Mater. 22 (2010) 957.
[21] C.R. Xia, W. Rauch, F. Chen, M.L. Liu, Solid State Ionics 149 (2002) 11.
[22] W.B. Wang, Z.J. Yang, H.T. Wang, G.L. Ma, W.J. Gao, Z.F. Zhou, J. Power Sources 196 (2011) 3539.
[23] G. Kresse, J. Hafner, Phys. Rev. B 48 (1993) 13115.
[24] M.W. Lufaso, R.B. Macquart, Y. Lee, T. Vogt, H.C.Z. Loye, J. Phys. Condens. Matter 18 (2006) 8761.
[25] A.B. Munoz-Garcia, D.E. Bugaris, M. Pavone, J.P. Hodges, A. Huq, F.L. Chen, H.C.Z. Loye, E.A. Carter, J. Am. Chem. Soc. 134 (2012) 6826.
[26] J.P. Perdew, K. Burke, M. Ernzerhof, Phys. Rev. Lett. 77 (1996) 3865.
[27] H.J. Monkhorst, J.D. Pack, Phys. Rev. B 13 (1976) 5188.
[28] W. Preis, E. Bucher, W. Sitte, Solid State Ionics 175 (2004) 393.
[29] X. Pan, Z.B. Wang, B.B. He, S.R. Wang, C.R. Xia, Int. J. Hydrogen Energy 38 (2013) 4108.
[30] A. Atkinson, S. Barnett, R.J. Gorte, J.T.S. Irvine, J. Mcevoy, M. Mogensen, S.C. Singhal, J. Vohs, Nat. Mater. 3 (2004) 17.
[31] S. Hashimoto, L. Kindermann, P.H. Larsen, F.W. Poulsen, M. Mogensen, J. Electroceram. 16 (2006) 103.
[32] S. Hui, A. Petric, Mater. Res. Bull. 37 (2002) 1215.
[33] J.A. Lane, J.A. Kilner, Solid State Ionics 136–137 (2000) 997.
[34] M.D. Segall, P.J.D. Lindan, M.J. Probert, C.J. Pickard, P.J. Hasnip, S.J. Clark, J. Phys. Condens. Matter 14 (2002) 2717.
[35] V.V. Gagulin, S.K. Korchagina, V.V. Ivanova, Y.A. Shevchuk, Inorg. Mater. 39 (2003) 625.
[36] Z.X. Xie, H.L. Zhao, Z.H. Du, T. Chen, N. Chen, X.T. Liu, S.J. Skinner, J. Phys. Chem. C 116 (2012) 9734.
[37] F. Tietz, Ionics 5 (1999) 129.
[38] D. Lee, J.H. Han, Y. Chun, R. Song, D.R. Shin, J. Power Sources 166 (2007) 35.
[39] Q. Liu, X. Dong, G. Xiao, F. Zhao, F. Chen, Adv. Mater. 22 (2010) 5478.
[40] L.L. Zhang, Q.J. Zhou, Q. He, T.M. He, J. Power Sources 195 (2010) 6356.
[41] G.L. Xiao, Q. Liu, X.H. Dong, K. Huang, F.L. Chen, J. Power Sources 195 (2010) 8071.
[42] G. Kim, M.D. Gross, W. Wang, J.M. Vohs, R.J. Gorte, J. Electrochem. Soc. 155 (2008) B360.
[43] T. Horita, K. Yamaji, N. Sakai, H. Yokokawa, A. Weber, E. Ivers-Tiffée, Solid State Ionics 138 (2000) 143.
[44] Q. Liu, D.E. Bugaris, G.L. Xiao, M. Chmarac, S.G. Ma, H. zur Loye, M.D. Amiridis, F.L. Chen, J. Power Sources 196 (2011) 9148.
[45] S.W. Tao, J.T.S. Irvine, J. Electrochem. Soc. 151 (2004) A252.
[46] C.R. Xia, F.L. Chen, M.L. Liu, Electrochem.Solid State Lett. 4 (2001) A52.
[47] T. Hibino, A. Hashimoto, M. Yano, M. Suzuki, M. Sano, Electrochim. Acta 48 (2003) 2531.